Metal-triggered changes in the stability and secondary structure of a tetrameric dihydropyrimidinase: A biophysical characterization

Sergio Martínez-Rodríguez [a,b,1], José A. Encinar [c], Estefanía Hurtado-Gómez [c], Jesús Prieto [d], Josefa M. Clemente-Jiménez [e], Francisco J. Las Heras-Vázquez [e], Felipe Rodríguez-Vico [e], José L. Neira [c,f,*,1]

[a] Laboratorium voor Ultrastructuur, Vrije Universiteit Brussels, Pleinlaan 2, B-1050 Brussels, Belgium
[b] Department of Molecular and Cellular Interactions, VIB, Pleinlaan 2, B-1050 Brussels, Belgium
[c] Instituto de Biología Molecular y Celular, Universidad Miguel Hernández, 03202 Elche, Alicante, Spain
[d] Structural Biology and Biocomputing Programme, Centro Nacional de Investigaciones Oncológicas (CNIO), 28007 Madrid, Spain
[e] Departamento de Química Física, Bioquímica y Química Inorgánica, Universidad de Almería, 04120 Almería, Spain
[f] Biocomputation and Complex Systems Physics Institute, 50009 Zaragoza, Spain

ARTICLE INFO

ABSTRACT

Dihydropyrimidinase is involved in the reductive pathway of pyrimidine degradation, catalysing the reversible hydrolysis of the cyclic amide bond (–CO–NH–) of 5,6-dihydrouracil and 5,6-dihydrothymine to the corresponding N-carbamoyl-β-amino acids. This enzyme is an attractive candidate for commercial production of D-amino acids, which are used in the production of semi-synthetic β-lactams, antiviral agents, artificial sweeteners, peptide hormones and pesticides. We have obtained the crystal structure of the dihydropyrimidinase from *Sinorhizobium meliloti* (SmelDhp) in the presence of zinc ions, but we have not been able to obtain good diffracting crystals in its absence. Then, the role of the ion in the structure of the protein, and in its stability, remains to be elucidated. In this work, the stability and the structure of SmelDhp have been studied in the absence and in the presence of zinc. In its absence, the protein acquired a tetrameric functional structure at pH~6.0, which is stable up to pH~9.0, as concluded from fluorescence and CD. Chemical-denaturation occurred *via* a monomeric intermediate with non-native structure. The addition of zinc caused: (i) an increase of the helical structure, and changes in the environment of aromatic residues; and, (ii) a higher thermal stability. However, chemical-denaturation still occurred through a monomeric intermediate. This is the first hydantoinase whose changes in the stability and in the secondary structure upon addition of zinc are described and explained, and one of the few examples where the zinc exclusively alters the secondary helical structure and the environment of some aromatic residues in the protein, leaving unchanged the quaternary structure.

1. Introduction

The amidohydrolase superfamily is formed by a set of enzymes catalyzing the hydrolysis of a wide variety of substrates including amide or ester functional groups at carbon and phosphorus atoms. Among them, cyclic amidohydrolases are involved in the hydrolysis of cyclic C–N bonds, and they are observed during the nucleotide metabolism of purine and pyrimidine. All the members of the family have a similar catalytic mechanism and they share the same TIM barrel scaffold [1,2]. Within this super-family, dihydropyrimidinases (EC 3.2.2.2) are involved in the reductive pathway of pyrimidine degradation catalysing the hydrolysis of 5,6-dihydrouracil and 5,6-dihydrothymine to 3-ureidopropionate and 3-ureidoisobutyrate (in this work, we adopt the recent convention, where the name hydantoinase is reserved for enzymes hydrolizing five-membered rings, and the name dihydropyrimidinase is used for enzymes able to hydrolize both five- and six-membered rings [3]). Dihydropyrimidinases have been found in diverse organisms, such as bacteria, animal, yeast and plants [4–8]. Several of these enzymes, with different stereoselectivities and substrate specificities, have been used in industrial bioconversion of optically pure D-amino acids with 5-monosubstituted hydantoins as substrates [9,10]. The D-amino acids, as unnatural chiral products, are important intermediates in the synthesis of various compounds, such as the semi-synthetic antibiotic β-lactams, antiviral agents, artificial sweeteners, peptide hormones and pesticides [11–13]. The increasing demand of D-amino acids by pharmaceutical and

biotechnological companies makes their enzymatic synthesis (*via* dihydropyrimidinases-hydantoinases) a process which has attracted much attention. Moreover, since several 5-monosubstituted hydantoins used in D-amino-acid production have a poor solubility, it is necessary to understand the structure and stability of such enzymes under a wide range of conditions, to find out where, and under which conditions, the enzyme remains active and the substrates more accessible.

We have embarked in the biochemical and structural characterization of the tetrameric 490-residues-long dihydropyrimidinase from *Sinorhizobium meliloti* CECT4114 (SmelDhp) [14]. We have previously solved the three-dimensional structure of SmelDhp by X-ray, only in the presence of the zinc ion [14] (PDB accession number 3DC8). In Fig. 1, we show the omit electron density and the $2F_o$–F_c maps of SmelDhp around the zinc ion pocket. It has been known for a long time that Zn^{2+} is necessary to proper activity of dihydropyrimidinase [1,2], but its effect on either the structure or stability of these enzymes has never been explained. Then, one of the aims of this work is to find out the effects of the ion on the structure and stability of SmelDhp. Here, we report the structure, stability and oligomerization state of SmelDhp at different pHs and temperatures, in the absence and in the presence of zinc ions, by using spectroscopic (namely, fluorescence, CD and FTIR) and hydrodynamic (size exclusion chromatography) techniques. Our results indicate that the native secondary structure of SmelDhp, formed by a similar percentage of α-helix and β-sheet, is present within a narrow pH range (from pH 6 to 9). Thermal denaturations were irreversible, within that narrow pH range, and the chemical folding reaction proceeds *via* a monomeric intermediate with non-native structure. Upon addition of 1 mM of Zn^{2+} the stability of the protein was enhanced, as concluded from the thermal- and chemical-denaturations; and most importantly: (i) only the percentage of secondary helical structure was increased; and, (ii) the environment of some aromatic residues modified. However, the chemical-denaturation reaction still proceeded through the same monomeric intermediate. To the best of our knowledge, this is the first dihydropyrimidinase whose changes in stability, and in the secondary and tertiary structures upon addition of zinc ions are extensively described and explained; further, it is one of the few examples where the presence of the ion selectively stabilizes one type of protein structure.

2. Materials and methods

2.1. Materials

All the chemicals were from Sigma (USA) and of the highest purity available. The molecular mass marker was from GE Healthcare (USA).

Ultra-pure urea and GdmCl were from ICN Biochemicals (USA). Exact concentrations of urea and GdmCl were calculated from the refractive index of the solutions [15]. Dialysis tubing with a molecular weight cut-off of 3500 Da was from Spectrapore (UK). Water was deionized and purified on a Millipore system.

2.2. Protein expression and purification

SmelDhp was expressed and purified as described [14]. The samples were extensively dialysed against water and stored at 193 K. A 20 μM protein stock solution was extensively dialyzed against 12 mM Tris (pH 7.5) with 1 mM $ZnCl_2$, to allow for ion binding. Protein concentration was calculated from the absorbance at 280 nm, by using the extinction coefficients of model compounds [16]. Centricon devices (Millipore) with a 10 kDa molecular weight cut-off were used to concentrate the protein. Samples for chemical-denaturations were prepared by dissolving the protein either in deionized water (unfolding) or in 7 M GdmCl (refolding). Protein absorbance was measured in a Shimadzu UV-1603 spectrophotometer (Japan).

2.3. Gel filtration chromatography

The standards used in calibration of the Superdex G200 HR 16/60 (GE Healthcare) column and their corresponding Stokes radii were: ovoalbumin (30.5 Å); bovine serum albumin (35.5 Å); aldolase (48.1 Å); ferritin (61 Å) and thyroglobulin (85 Å) [17,18]. These values allow us to determine the hydrodynamic radius, R_s, of a protein [19,20]. The bed and the void volumes were determined by using riboflavin and blue-dextran, yielding 23.65 and 7.01 ml, respectively. Samples were loaded in 25 mM Tris (pH 7.3) with 150 mM NaCl, at 1 ml/min and running on an AKTA-FPLC system (GE Healthcare) at 298 K, with an on-line detector at 280 nm.

The buffers in the pH-denaturation experiments (see below) were used at a final concentration of 50 mM, with 150 mM of NaCl to avoid column interactions. Each measurement was repeated three times with new samples at 2 μM of protein (in protomer units); in the following, protein concentrations will be expressed in protomer units. The protein concentration ranged from 2 to 76.5 μM during the protein-concentration experiments.

2.4. Differential scanning calorimetry

DSC experiments were performed in a MicroCal MC-2 differential scanning calorimeter interfaced with a computer equipped with a Data
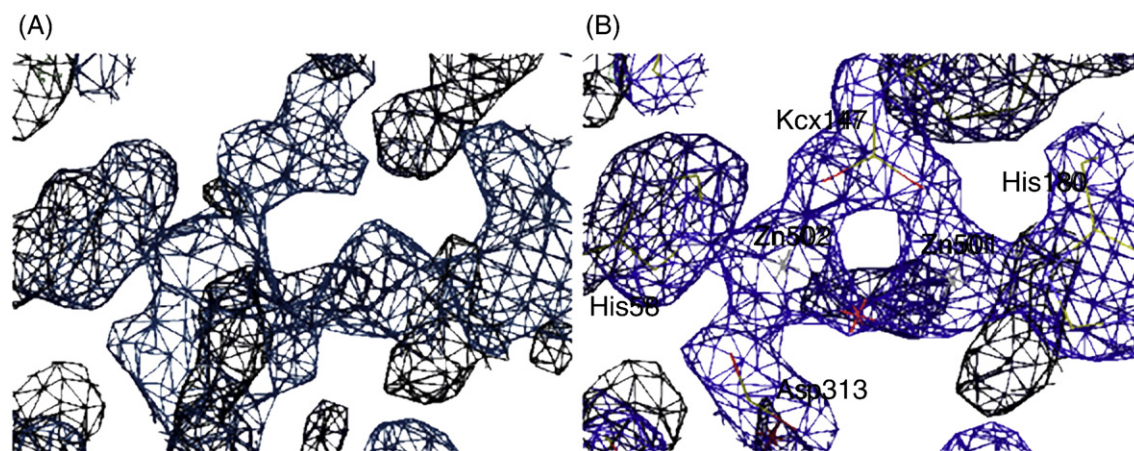
Fig. 1. Electron densities during the refining process of the X-ray structure of SmelDhp. (A) Simulated omit electron density map at 1.0 σ contours, generated by shaking the structure by 0.5 Å with MOLEMAN2, removing chain A from the model, and refining 20 cycles with REFMAC5. (B) The $2F_o$–F_c map at 1.0 σ contours after several cycles of refinement, including several residues in the proximity of the binuclear Zn-centre. Figure orientation is roughly the same as in (A). Kcx indicates a carboxylated lysine. Both figures were directly obtained from COOT program (defining the background as transparent with Microsoft word).

Translation DT-2801 A/D converter board for instrument control and automatic data collection. Protein was dialysed twice against 2 l of 10 mM MES buffer, 200 mM NaCl (pH 6.5) at 278 K. Calorimetric experiments were performed at concentrations of 0.4 (7.5 μM) and 0.8 mg/ml (15 μM); the protein was irreversibly unfolded in all cases. Samples were heated at a constant scan rate of 30, 45, 60 and 90 K/h and held under a constant external pressure of 1 bar to avoid bubble formation and evaporation at temperatures above 368 K. In all cases, the large broadness of the DSC profiles (Fig. 2 of Supplementary Material) indicated that the shape was not consistent with a two-state irreversible model with first-order kinetics, thus hampering kinetic studies. Since the thermal midpoint was scan-rate dependent, it was necessary to correct for the finite time response of the instrument [21–23]. The corrected and non-corrected traces in the absence of the ion were virtually identical (data not shown). The calorimetric midpoint was determined as described if a proper unfolding baseline was observed [21–23]. Experiments in the presence of Zn^{2+}, led to a highly distorted unfolded baseline due to a massive precipitation, and then a reliable determination of the calorimetric midpoint and C_p could not be carried out.

Before rescanning, the samples were cooled down *in situ* to 293 K for 40 min. Experimental data were corrected from small mismatches between the two cells by subtracting a buffer *versus* buffer baseline, prior to data analysis. After normalising to concentration, a chemical baseline calculated from the progress of the unfolding transition was subtracted.

2.5. Fluorescence measurements

Fluorescence spectra were collected on a Cary Varian (USA) spectrofluorimeter, interfaced with a Peltier unit, at 298 K. The SmelDhp concentration in the pH- or chemical-denaturation experiments was 2 μM, unless it is stated, and the final concentration of the buffer was 10 mM. A 1-cm-pathlength quartz cell (Hellma) was used.

(a) *Steady state spectra*: Protein samples were excited at 280 and 295 nm to characterize a different behaviour of tryptophan and tyrosine residues [24]. The slit widths were 5 nm for the excitation and emission light. The fluorescence experiments were recorded between 300 and 400 nm. The signal was acquired for 1 s and the wavelength increment was set to 1 nm. Blank corrections were made in all spectra.
The pHs of samples were measured after completion of the experiments with a thin Aldrich electrode in a Radiometer (Copenhagen) pH-meter. The salts and acids used were: pH 2.0–3.0, phosphoric acid; pH 3.0–4.0, formic acid; pH 4.0–5.5, acetic acid; pH 6.0–7.0, NaH_2PO_4; pH 7.5–9.0, Tris acid; pH 9.5–11.0, Na_2CO_3; pH 11.5–12.0, Na_3PO_4.

(b) *ANS-binding*: Excitation wavelength was 380 nm, and emission was measured from 400 to 600 nm. Slit widths were 5 nm for excitation and emission light. Stock solutions of ANS (1 mM) were prepared in water and diluted to yield a final concentration of 100 μM. Blank solutions were subtracted from the corresponding spectra.

2.6. Circular dichroism measurements

Circular dichroism spectra were collected on a Jasco J810 spectropolarimeter (Japan) fitted with a thermostated cell holder and interfaced with a Peltier unit. The instrument was periodically calibrated with (+) 10-camphorsulphonic acid. Protein concentration was 2 μM in all cases, unless it is stated.

(a) *Steady-state spectra*: Isothermal wavelength spectra were acquired at a scan speed of 50 nm/min with a response time of 4 s and averaged over four scans, at 298 K. Far-UV measurements were carried out at 2 μM of protein, 10 mM of the corresponding buffer (see above), in a 0.1-cm-pathlength cell. Every pH-denaturation experiment was repeated three times with new samples. Near-UV measurements were carried out with a concentration of 15–20 μM of protein, in a 0.5-cm-pathlength cell. Molar ellipticity, [Θ], was obtained from raw ellipticity data, Θ, according to: $[Θ] = / (10lcN)$, where l is the pathlength cell, c the concentration (in M), and N the number of amino acids. In the chemical-denaturation experiments, far-UV CD spectra were acquired with a scan speed of 50 nm/min; four scans were recorded and averaged, with a response time of 4 s, at 298 K. Spectra were corrected by subtracting the proper baseline. Chemical denaturations were repeated three times with new samples.

(b) *Thermal denaturation experiments*: Thermal denaturation experiments were performed at heating rates of 60 K/h and a response time of 8 s. Thermal scans were collected in the far-UV region at 222 nm in 0.1-cm-pathlength cells. The conditions were the same as those reported in the steady-state experiments. The possibility of drifting of the spectropolarimeter was tested by running two samples containing buffer, before and after the thermal experiments. No difference was observed between the scans.

2.7. Analysis of the pH- and chemical-denaturation curves, and free energy determination

The average emission intensity, $<\lambda>$, in fluorescence spectra was calculated as described [25].

The pH-denaturation experiments were analysed assuming that both species, protonated and deprotonated, contributed to the spectrum:

$$X = \frac{\left(X_a + X_b 10^{n(pH-pK_a)}\right)}{\left(1 + 10^{n(pH-pK_a)}\right)}, \tag{1}$$

where X is the physical property observed (ellipticity, fluorescence intensity or $<\lambda>$), X_a is that observed for the acidic region, X_b is that at high pHs, pK_a is the apparent pK of the titrating group, and n is the Hill coefficient. The apparent pK_a was obtained from three different measurements, prepared with new samples. Fitting to Eq. (1) by non-linear least-squares analysis was carried out by using Kaleidagraph (Abelbeck software) on a PC computer.

We firstly used urea as the chemical-denaturant agent (to avoid any electrostatic effect caused by the GdmCl), but no sigmoidal behaviour was observed at any of the explored pHs (data not shown). Thermal- and GdmCl-chemical denaturation data were analysed using a concentration-dependent two-state folding mechanism as described [26]; attempts to fit to a three-state folding mechanism did not improve either the regression coefficient or the residuals (data not shown). Fitting was carried out by using Kaleidagraph (Abelbeck software) on a PC computer.

2.8. Fourier transform infrared spectroscopy

The protein was lyophilised and dissolved in deuterated buffer at the desired pH; no pH-corrections were done for the isotope effects. Samples of SmelDhp, at a final concentration of 125 μM, were placed between a pair of CaF_2 windows separated by a 50 μm thick spacer, in a Harrick demountable cell. Spectra were acquired on a Bruker FTIR instrument equipped with a DTGS detector and thermostated with a Braun water bath at the desired temperature. The cell container was filled with dry air.

(a) *Steady-state spectra*: Five-hundred scans per sample were taken, averaged, apodized with a Happ–Genzel function, and Fourier transformed to give a final resolution of 2 cm^{-1}. The signal to noise ratio of the spectra was better than 10,000:1. Buffer contributions
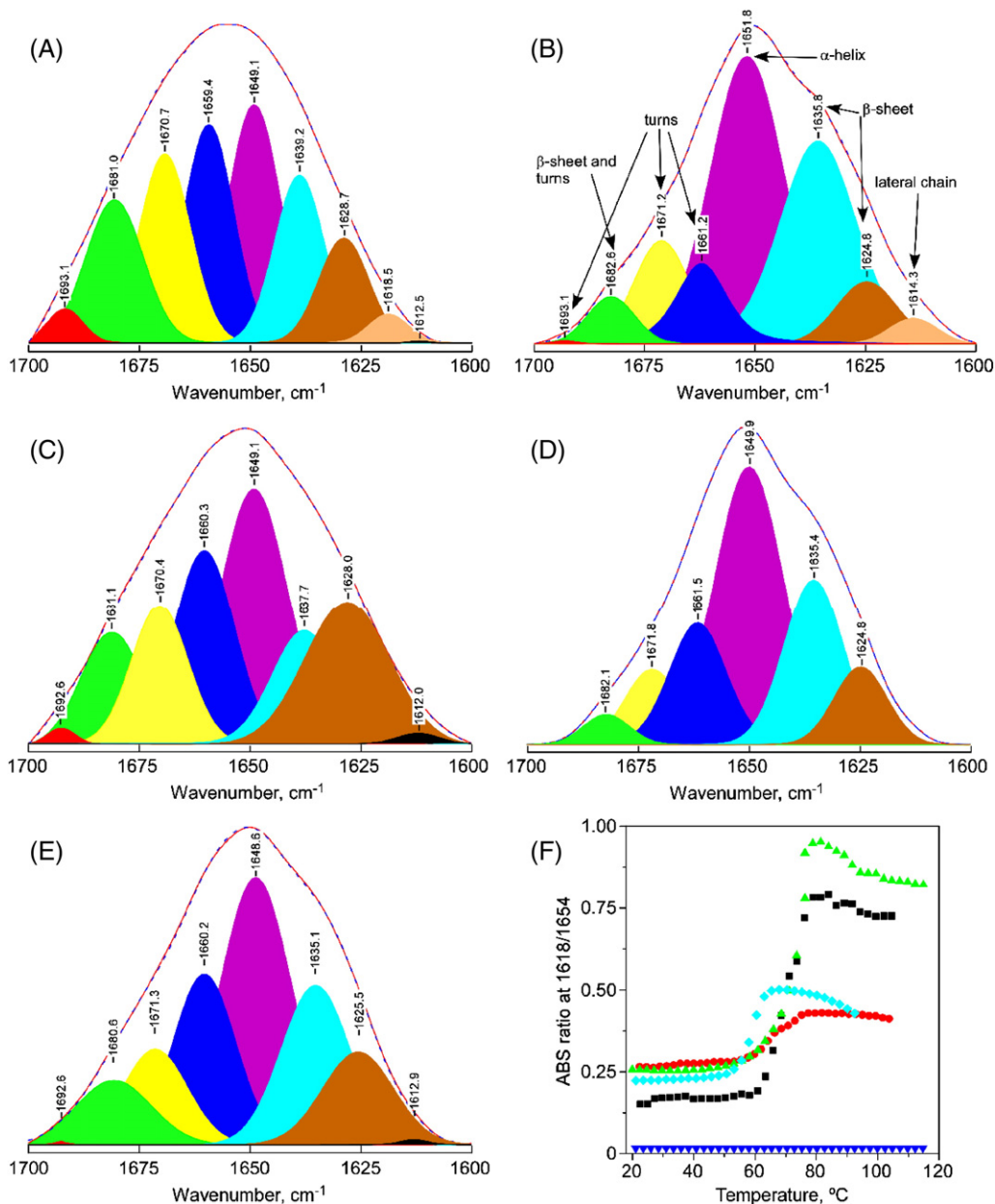
Fig. 2. FTIR spectra and thermal denaturations of SmelDhp at selected pHs in the absence and in the presence of 1 mM Zn^{2+}. Amide I′ band fitting analysis of SmelDhp in the absence (A, C, E) and in the presence (B, D) of 1 mM Zn^{2+} at 298 K pHs 2.5 (A, B), 7.0 (C, D) and 12.0 (E). These panels indicate: (i) band decomposition of the spectra in D_2O buffer (the component bands are shown with different coloured areas, and with arrows in one of the panels); (ii) the envelope (red continuous line); and, (iii) the reconstruction of the Amide I′ band from the components (dashed lines). Note that the dashed and continuous lines are virtually superimposed, because of the goodness of the fit, and therefore they are hard to distinguish. The F panel shows the temperature-dependence of the ratio absorbance at 1618/1654 (cm^{-1}) for SmelDhp at pH 2.5 (without Zn^{2+}, purple inverted triangles; and with 1 mM Zn^{2+}, light green triangles), pH 7.0 (without Zn^{2+}, red circles; and with 1 mM Zn^{2+}, black squares) and pH 12.0 (without Zn^{2+}, light blue diamonds). Fitting of data to the two-state model [26] leads to: pH 7: 338.6±0.2 K (without Zn^{2+}); 343.6±0.1 K (with Zn^{2+}); pH 2.5: no transition in the absence of Zn^{2+}, 346.6±0.5 K (with Zn^{2+}); pH 12.0: 332.5±0.2 K (without Zn^{2+}).

were subtracted, and the resulting spectra were used for analysis. Fourier self-deconvolution of infrared spectra of SmelDhp at pH 2.5 shows the following peaks: 1693.0, 1680.7, 1669.4, 1660.4, 1649.1, 1639.2, 1628.7, 1618.5, 1612.5 cm^{-1}. Band decomposition of the original Amide I′ have been described previously [27]. Briefly, for each component, four parameters are considered: band position, band height, bandwidth, and band shape. Thus, in a typical Amide I′ band decomposition with six or seven band components, the number of parameters is 24–28. The number and position of component bands is obtained through deconvolution and derivation, initial heights are set to 90% of those in the original spectrum for the bands in the wings and for the most intense component; and to 70% of the original intensity for the other

bands. Initial bandwidths are estimated from the Fourier derivative. The Lorentzian component of the bands is initially set at 10%. The baseline is removed prior to starting the fitting process. The iteration procedure is carried out in two steps as described in the last reference cited above. The mathematical solution of the decomposition may not be unique, but if restrictions are imposed, such as: (a) the maintenance of the initial band positions in an interval of ±2 cm^{-1}; (b) the preservation of the bandwidth within the expected limits; or, (c) the agreement with theoretical boundaries or predictions, the result becomes, in practice, unique. The fitting result is then evaluated: (a) by overlapping the reconstituted overall curve on the original spectrum; and, (b) by examining the residuals obtained by subtracting the fitting from
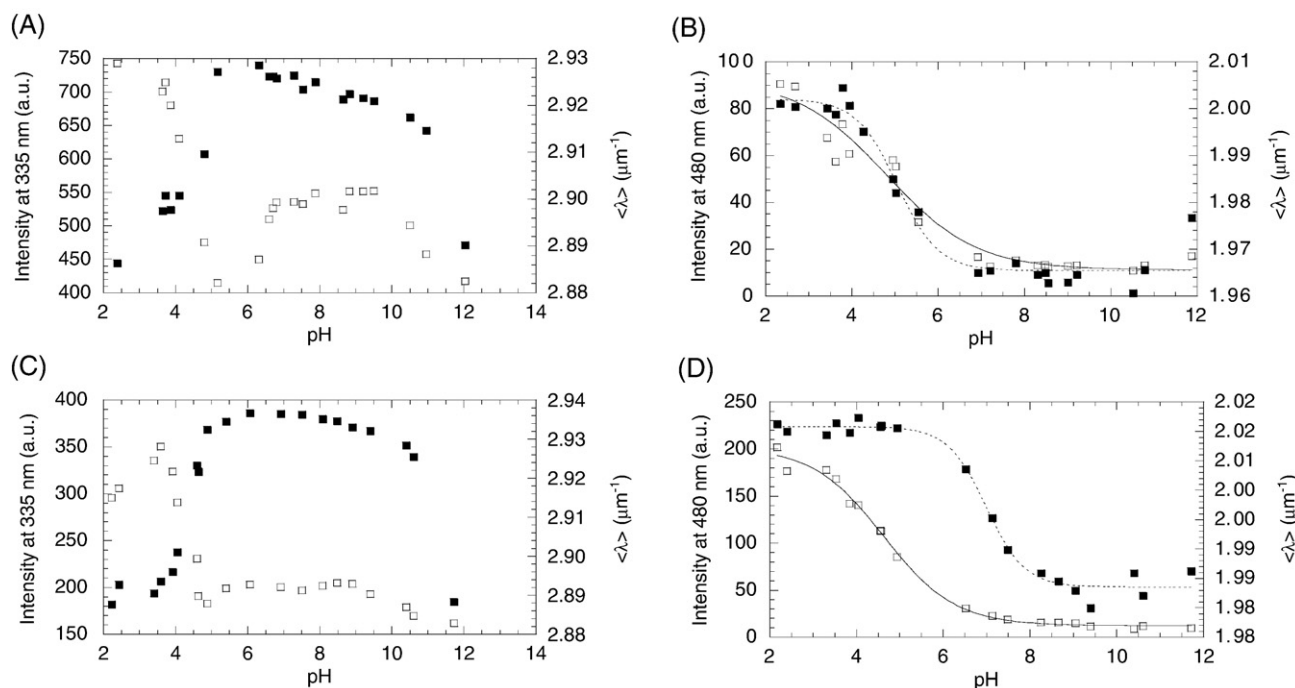
Fig. 3. pH-induced structural changes of SmelDhp followed by fluorescence. (A) Changes followed by the intrinsic protein fluorescence, monitoring the <λ> (filled squares, right axis) and the intensity at 335 nm (blank squares, left axis) in the absence of Zn^{2+}. (B) Changes followed by ANS fluorescence, monitoring the <λ> (filled squares, right axis, dotted line) and the intensity at 480 nm (blank squares, left axis, continuous line) in the absence of Zn^{2+}. (C) Changes followed by the intrinsic protein fluorescence, monitoring the <λ> (filled squares, right axis, blank squares, left axis) in the presence of 1 mM Zn^{2+}. (D) Changes followed by ANS fluorescence, monitoring the <λ> (filled squares, right axis, dotted line) and the intensity at 480 nm (blank squares, left axis, continuous line) in the presence of 1 mM Zn^{2+}. The lines are the fitting of data to Eq. (1). The temperature was 298 K, and protein concentration was 2 μM.

the original curve. The error in estimation of the percentage of secondary structure depends mainly on the removal of spectral noise, which was estimated to be 5% [27]. In the experiments with Zn^{2+}, the corresponding volume of a stock solution of $ZnCl_2$ was added, and the sample lyophilized.

(b) *Thermal denaturation measurements*: The samples were submitted to heating cycles. Each step in the cycles include: (i) a step-like increase in temperature; (ii) a stabilization period of the sample in the cell at each temperature; and, (iii) a period of spectral acquisition. The duration of a complete heating cycle was ~2.5 h, in which the temperature was increased by approximately 5 K steps every 13 min. Fifty scans *per* temperature were averaged. Protein thermal denaturation can be monitored by FTIR by following the changes induced in the amide I′ band by temperature. Protein denaturation is characterized in D_2O by the appearance of two bands around 1620 and 1685 cm^{-1}, which are the result of intermolecular protein–protein contacts. Different plots can be used to characterize the thermal profile, e.g., bandwidth *versus* temperature, or the ratio (absorbance of the most intense component/absorbance of the emerging band) *versus* temperature. The thermal midpoint, T_m, was determined by using a two-state folding mechanism [26] following the changes in the ratio at two wavelengths; fittings to a three-state folding mechanism did not improve either the regression coefficient or the residuals (data not shown).

3. Results

3.1. Structure of SmelDhp in the absence and in the presence of Zn^{2+}

3.1.1. Structure of SmelDhp at different pHs

We used several spectroscopic probes to monitor the conformational changes in the absence and in the presence of 1 mM Zn^{2+}, as the pH varied.

(a) *FTIR*: The secondary structure of SmelDhp was examined at three different pHs (2.5, 7.0 and 12.0) (Fig. 2) by band fitting analysis of amide I′. In the absence of Zn^{2+}, the percentages of α-helix increased as the pH was raised, from 20% to acidic pH to a 33% to basic pH (Fig. 2 A, C, E). Conversely, the components assigned to turns diminished when the pH increased. The components of β-structure remained basically unaltered (~25%).

At pH 12.0, the Zn^{2+} and/or the protein precipitated, hampering any structural characterization. At acidic and neutral pHs, the presence of Zn^{2+} caused an increase in the percentage of α-helix at the expense of turns: for instance, at pH 7.0 the α-helix increased from 27% to 41%. Furthermore, these samples had residual amide II (1547 cm^{-1}), which showed hydrogen-exchange (Fig. 1 of Supplementary Material). This behaviour is characteristic of stable helical structure [28]. We can compare the percentages of secondary structure with those from the X-Ray structure (3DC8): 20.1% (β-strand), 32.4% (α-helix), 2.9% (3_{10}-helix) and 44.6% (other types of structure), at pH 4.6, where the structure was solved [14]. These results compare reasonably well (41% for the α-helix at pH 7.0, Fig. 2 D) with the FTIR results, with the small changes probably due to the different pHs.

(b) *Intrinsic fluorescence spectroscopy*: We used fluorescence to monitor changes in the tertiary structure of the protein around the eight tryptophans and the eleven tyrosines. The emission fluorescence spectra of SmelDhp whether or not the ion was present had maxima at 335 nm at neutral pHs, and then, they were dominated by the emission of the tryptophan residues. From the blue-shifted maxima, we can conclude that the tryptophans (or at least one of them) are completely buried in the structure, either zinc is present or not. As the pH varied, the maxima wavelengths of the spectra were red-shifted towards 346 nm, suggesting that some, if not all, of the fluorescent
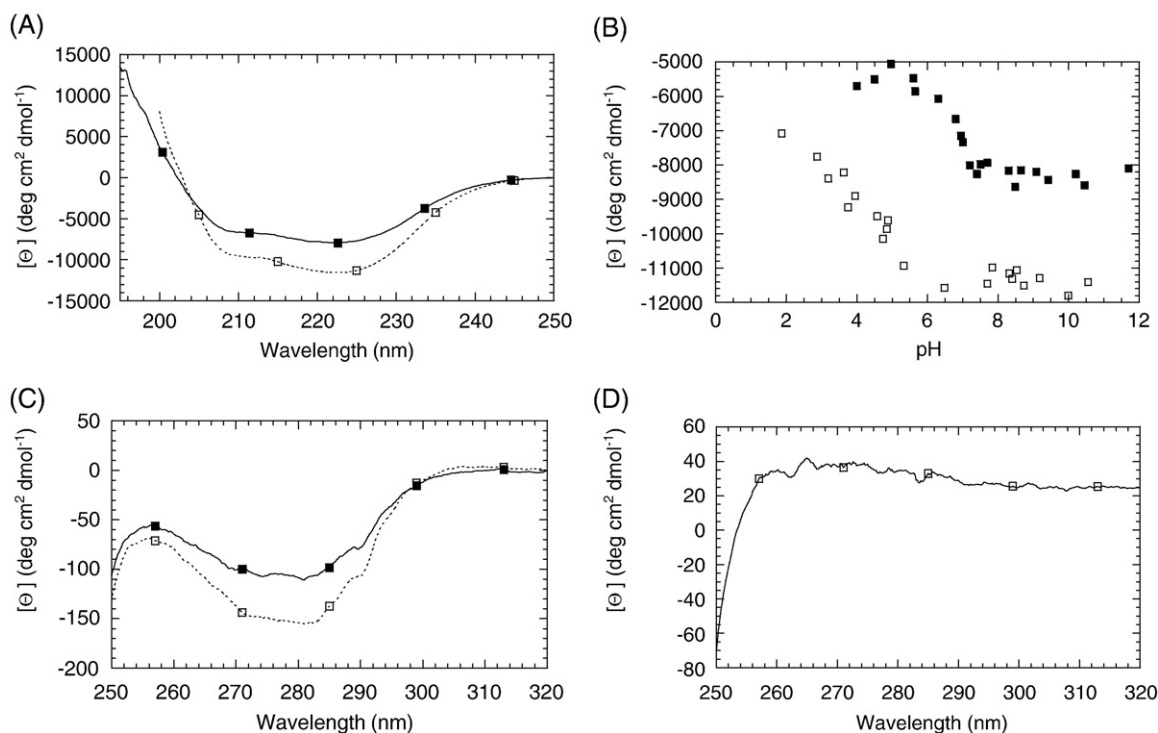
Fig. 4. pH-induced structural changes of SmelDhp followed by CD. (A) Far-UV steady-state spectra in the absence (filled squares, continuous line) and in the presence of 1 mM Zn^{2+} (blank squares, dotted line) at pH 7.0. (B) Changes in the $[\Theta]$ at 222 nm as the pH varied in the presence (blank squares) and in the absence (filled squares) of 1 mM Zn^{2+}. (C) Near-UV steady-state spectra in the absence (filled squares, continuous line) and in the presence of 1 mM Zn^{2+} (blank squares, dotted line) at pH 7.0. (D) Near-UV CD steady-state spectrum in the absence of Zn^{2+} at pH 1.75. The temperature was 298 K.

aromatic residues were solvent-exposed (data not shown). The maxima wavelengths did not change from 0.5 to 5 µM (data not shown) either in the presence or in the absence of Zn^{2+}.

In the absence of the ion, the intensity at 335 nm (either by excitation at 280 or 295 nm) showed three titrations: one at acidic pH, another one close to physiological pHs, and the last at basic pHs (Fig. 3 A, blank squares). The pK_a of the titration at acidic pH was 4.70±0.04. The second one, which partially overlapped with the first, had an apparent pK_a close to 6.0, similar to that observed for solvent-exposed histidine residues [29]. Finally, we could not determine the pK_a of the titration at high pH, which is probably related to the deprotonation of some, if not all, of the tyrosine, arginine or lysine residues [29]. The profile of $<\lambda>$ versus pH shows only two titrations at low and high pH at 280 or 295 nm (Fig. 3 A, filled squares). The apparent pK_a of the titration at low pH was 4.79±0.04, similar to that observed in the intensity at 335 nm. The pK_a of the basic transition, on the other hand, could not be determined.

On the other hand, in the presence of the ion, both parameters showed only two titrations (Fig. 3 C): one at acidic pH and other at basic pHs. The pK_a of the titration at low pH was 4.38±0.04 (either by the $<\lambda>$ or the intensity at 335 nm), similar to that observed in the absence of the ion.

(c) *ANS-binding*: ANS-binding was used to monitor the solvent-exposed hydrophobic regions [30]. At low pHs either the ion was present or not, the fluorescence intensity at 480 nm was large, and decreased as the pH was raised (Fig. 3 B, blank squares). The intensity at 480 nm showed a sigmoidal behaviour whether or not metal was present, with a pK_a=4.8±0.3 (no Zn^{2+}) (Fig. 3 B, blank squares) or 4.62±0.07 (in the presence of Zn^{2+}) (Fig. 3 D, blank squares). Conversely, the behaviour of $<\lambda>$ showed a titration with a pK_a=5.0±0.1, in the absence of the metal (Fig. 3 B, filled squares), and when the metal was present the pK_a was 6.98±0.08, (Fig. 3 D, filled squares).

(d) *Far and near-UV*: The far-UV at physiological pH either in the absence or in the presence of the metal was characterized by the presence of minima at 208 and 222 nm (Fig. 4 A). In the presence of Zn^{2+}, the ellipticities were larger in absolute value at 222 (at 222 nm, the intensity was 1.45-times larger), suggesting a higher percentage of secondary structure. However, it is important to keep in mind that aromatic residues absorb at 222 nm [31,32]. The spectral shape did not change under both conditions in the concentration range from 1 to 8 µM, suggesting that the structure and the oligomerization state of the protein were not modified (data not shown). The ellipticity at 222 nm in the absence of the ion showed a pH-denaturation sigmoidal behaviour (Fig. 4 B, filled squares), with a pK_a=6.8±0.1, similar to the value obtained by following the changes in ANS (see above). We could not determine the pK_a of the titration in the presence of the metal (Fig. 4 B, blank squares).

Near-UV spectra gives information on the asymmetric and rigid environment of the aromatic residues [31,32]. The near-UV of SmelDhp was very intense: it has a broad minimum centered at 280 nm, and another shallow one at 290 nm (Fig. 4 C, filled squares), suggesting a very intense L_b transition of the trypto-phans [33,34]. In the presence of the ion, the spectrum is more intense (Fig. 4 C, blank squares), suggesting changes in the asymmetric environment of the aromatic residues. The changes were 1.43-times larger than in the absence of Zn^{2+}, similar to the numbers obtained in the FTIR and far-UV CD (see above). All these features disappeared at pH 1.75 whether or not the ion was present (Fig. 4 D), indicating that at low pHs the environment of aromatic residues was not longer asymmetric, and then, the protein was unfolded.

(e) *Gel filtration measurements*: In the absence of the ion, SmelDhp eluted at 10.96 ml at pH 7.0, which yields a R_s of 47.5 Å [19,20] (Fig. 5 A). The theoretical R_s for an anhydrous tetrameric sphere is 39.5 Å, smaller than that obtained experimentally; the
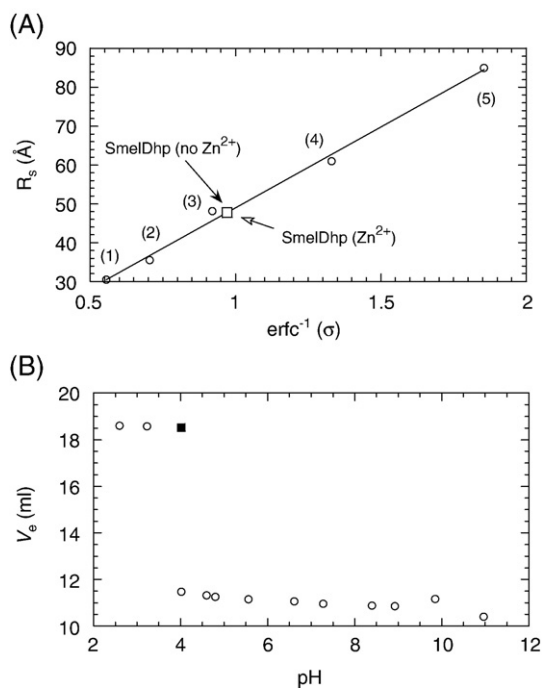
Fig. 5. Hydrodynamic properties of SmelDhp as monitored by size exclusion chromatography. (A) Determination of the Stokes radius of SmelDhp at pH 7.0. The elution volume of the protein in the absence of Zn^{2+} is indicated by a filled arrow head, and that in the presence of Zn^{2+} by a blank arrow head. The numbering corresponds to the elution volumes of ovalbumin (1), albumin (2), aldolase (3), ferritin (4) and thyroglobulin (5). The equation was: $R_s = 41.6 \times \mathrm{erfc}^{-1}(\sigma) + 7.39$ (with a regression coefficient of 0.99). (B) Changes in the V_e of SmelDhp with the pH in the absence of Zn^{2+}. The buffers were those used in the other spectroscopic techniques plus 150 mM NaCl to avoid interactions with the column. Protein concentration was 2 μM and temperature was 298 K. The filled square indicates the second elution peak observed at pH 4.0.

discrepancy is probably due to the oblong molecular shape of the protein (PDB number: 3DC8). We also used the more common correlation between the molecular weight and V_e [35], yielding a molecular weight of 244815 Da, half-way between that of a tetrameric and pentameric SmelDhp species (data not shown). In the presence of the ion, the V_e was the same, and then, it yields the same R_s (Fig. 5 A, blank arrow). We also observed a sigmoidal behaviour during the pH-denaturation (Fig. 5 B). Either in the absence or in the presence of the ion, at pH < 4.0, the protein eluted at 18.52 ± 0.03 ml, close to the bed volume (23.65 ml); at pH = 4.0, two peaks appeared at 11.47 ml and 18.52 ml. Calculation of the R_s with a V_e of 18.52 ml, led to unreal values for either the R_s or the molecular weight (data not shown); then, we suggest that the large observed V_e at low pHs was probably due to protein-column interactions. Further, we can rule out that this low-pH species is an unfolded tetrameric form, since a completely unfolded oligomeric protein should appear at the void volume (7.01 ml). Finally, at pH > 4.0, a single peak with $V_e \sim 10.96$ ml appeared.

In conclusion, the presence of the ion increased the secondary structure (far-UV and FTIR) and induced changes in the aromatic environment of several residues (near-UV), but it did not change the quaternary structure of the protein nor its compactness (gel-filtration).

3.2. Stability of SmelDhp in the absence and in the presence of Zn^{2+}

On the basis of the spectroscopic results described above, several questions can be raised: how stable is the native structure acquired above pH 6.0 whether or not the ion was present?; and, although

SmelDhp does not acquire a native structure up to pH 6.0, have the species at low pH a well-folded conformation whether or not the ion is present?, in the presence of Zn^{2+} does the increment in secondary structure result in an increase of protein stability? To address those questions, we carried out thermal- and chemical-denaturations, either in the presence or in the absence of the ion.

(a) *Thermal denaturations*: Thermal denaturations whether or not the ion was present, were followed by CD, FTIR and DSC at several pHs. The thermal reactions in all cases were irreversible since: (i) the native CD and FTIR signals were not recovered after heating; and, (ii) no endotherm was observed in the second DSC scan. Thus, we did not try to estimate the thermodynamic parameters, governing thermal unfolding, but we could determine the T_m, as it has been described in other proteins showing irreversible thermal denaturations [21–23]. The CD and DSC scans were not concentration-dependent, whether the ion was present or not: the T_ms were 336.94 K at 7.5 μM and 337.13 K at 15.0 μM (at pH 7.0) in DSC; and the T_ms ranged from 338.1 ± 0.2 K at 2 μM to 337.5 ± 0.4 K at 5 μM of protein (at pH 7.0) in the thermal-CD denaturations (or from 343.5 K at 2 μM to 342.8 K at 5 μM of protein, in the presence of the ion). Similar T_ms were observed in the FTIR experiments: 338.6 K, at pH 7.0, where the concentration was 120 μM (Fig. 2 F). In the absence of the ion, the T_ms (measured either by CD or DSC) showed a bell-shaped behaviour above pH 4.0 (Fig. 6 A), with a maximum at pH 7.0. No sigmoidal transitions were observed at pH < 3.0, except when the ion was present (Fig. 2 F), probably due to the presence of partially folded conformations. We could not carry out a kinetic analysis of the irreversible process since the shape of the DSC profile suggest that the thermal denaturation does not follow a two-state irreversible model (Fig. 2 of Supplementary Material). The T_ms in the presence of Zn^{2+} also showed a bell-shaped tendency (Fig. 6 A, filled circles), and they were consistently
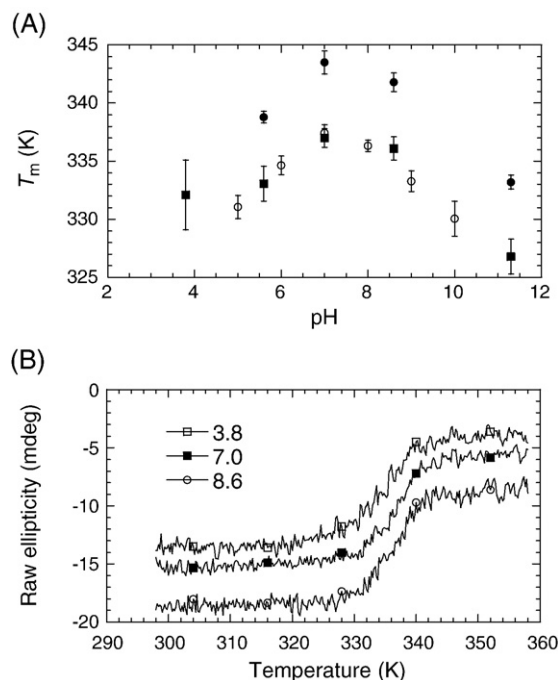
Fig. 6. Stability of SmelDhp at several pHs as determined by thermal denaturations. (A) The T_ms at several pHs as determined by DSC (corrected by the response time, blank circles) and CD (filled squares) in the absence of Zn^{2+}; and as determined by CD (filled circles) in the presence of the ion. The error bars are fitting errors to the two-state model [26]. (B) Thermal denaturation scans monitored by the changes in ellipticity at 222 nm at several pHs in the absence of Zn^{2+}. The y-axis units are arbitrary, and the traces have been scaled up for the sake of clarity.
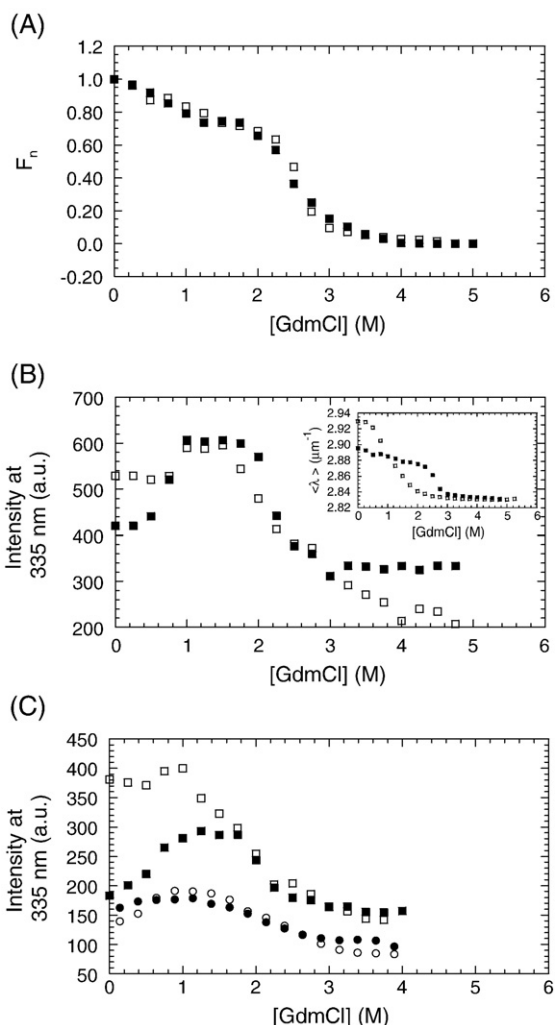
Fig. 7. Stability of SmelDhp at several pHs as determined by GdmCl-denaturations in the absence of Zn^{2+}. (A) Fraction of native molecules (calculated as $F_N=(X-X_D)/(X_N-X_D)$, where X_N and X_D are the corresponding fractions of the folded and unfolded states, respectively; and X is the physical property (ellipticity or $<\lambda>$, after excitation at 280 nm). Fluorescence (filled squares) and CD (blank squares) data were acquired at 2 μM of protein concentration. (B) The intensity at 335 nm (after excitation at 280 nm) at pH 8.3 (blank squares) and pH 5.4 (filled squares) at 2 μM. Inset: The $<\lambda>$ after excitation at 280 nm at the same pHs, with the same symbols for both pHs. (C) The intensity at 335 nm (after excitation at 280 nm) in the unfolding experiments at 0.9 μM (blank squares) and 2 μM (filled squares); and at 0.9 μM (blank circles) and 2 μM (filled circles) in the refolding experiments. All experiments were acquired at 298 K and pH 7.0.

higher than those in the absence of the ion (by ~6 K at any pH, Fig. 6 A).

(b) *Chemical denaturations*: Upon addition of GdmCl to SmelDhp, whether or not Zn^{2+} was present, we observed a shift in the emission maximum from 335 to 350 nm. Further, the ellipticity at 222 nm also decreased (Fig. 7 A, blank squares; Fig. 8 B), suggesting that the loss of tertiary (fluorescence) and secondary (CD) structure occurred concomitantly. The denaturation-curves monitored by fluorescence or CD showed two transitions whether or not the ion was present: one at low [GdmCl], and other at concentrations ~2.4 M of GdmCl (Figs. 7A and 8A). In the absence of the ion, the first transition was clearly observed by following the changes in the ellipticity at 222 nm (Fig. 7 A, blank squares), and in the intensity at 335 nm (Fig. 7 B, main panel; Fig. 8 A, blank squares), but it was obscured when the $<\lambda>$ was monitored (Fig. 7 B, inset; Fig. 8 A, filled squares). In the absence of the ion, the first transition was pH- (Fig. 7 B, main panel) and concentration-dependent (Fig. 7 C, squares),

although the midpoint could not be determined very precisely at some of the low protein concentrations used. These results suggest that the first transition probably involved oligomer dissociation under both conditions. At pH 7.0 in the absence of ion, a $[GdmCl]_{1/2}=0.6\pm0.1$ M was observed at 2 μM of protein (Fig. 7 C, filled squares), but no clear transition was observed at 0.9 μM (Fig. 7 C, blank squares); whereas, at pH 8.3, a $[GdmCl]_{1/2}=0.81\pm0.08$ M, at 2 μM of protein, was obtained (Fig. 7 B, filled squares, main panel). In the presence of the ion, this transition was also concentration-dependent, but its tendency and intensity were different (Fig. 8 A), suggesting changes in the dissociation behaviour of SmelDhp. Under both conditions, this first transition was not reversible (Fig. 7 C, and data not shown) and, then, we did not try to obtain any thermodynamic parameter. Conversely, the second transition, was reversible (Fig. 7 C), concentration-independent, within the protein concentration range explored (0.8 to 2 μM), and with similar thermodynamic parameters under both conditions (Fig. 8 and Table 1) suggesting that it involves unfolding of a monomeric species. Furthermore, the transition was pH-independent.

In conclusion, the presence of Zn^{2+} did not only increase the percentage of secondary structure, but also the thermal and chemical stability of SmelDhp. This stabilization is probably due to metal binding.

4. Discussion

4.1. Zinc ions stabilise the tetrameric structure of SmelDhp

Metals perform a variety of tasks in cells from structural stabilization to enzyme catalysis, activating key life processes such as respiration and photosynthesis [36,37]. The Na, K, Mg, Ca, Zn, Cu, Fe, Co and Mn are the most frequently observed in proteins under
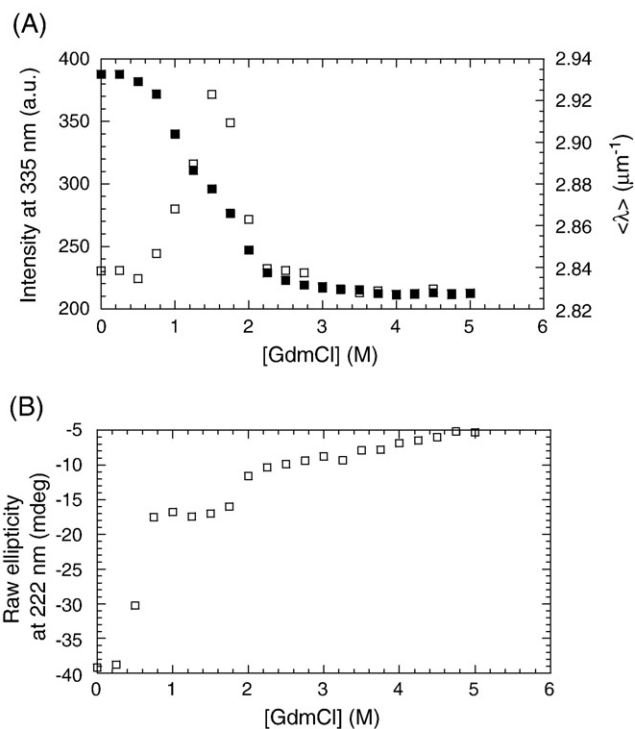
Fig. 8. Stability of SmelDhp at several pHs as determined by GdmCl-denaturations in 1 mM of Zn^{2+}. (A) The $<\lambda>$ (filled squares, right axis) and the intensity at 335 nm (blank squares, left axis) after excitation at 280 nm, at pH 7.0. (B) Changes in the ellipticity at 222 nm, at pH 7.0. Data were acquired at 2 μM of protein concentration.

Table 1
Thermodynamic parameters of the concentration-independent transition of SmelDhp in the absence of Zn^{2+}

pH	m (kJ mol^{-1} M^{-1})	[GdmCl]$_{1/2}$ (M)
5.4	16±4	2.32±0.04
5.7	18±3	2.26±0.02
6.5	18±6	1.9±0.2
7.0	16±3	2.0±0.1
8.1	17±6	1.9±0.1
9.3	18±2	1.90±0.09

Experiments were carried out at 298 K. The values shown were obtained by following the changes in intensity at 335 nm after excitation at 280 nm (similar results were obtained by excitation at 295 nm).

physiological conditions; and among those, Zn plays essential roles as cofactor of metabolic enzymes and transcription factors. Zinc is well-suited for its role in protein structure because: (i) it is a borderline acid, and then, it can interact with ligands; (ii) it is not redox-active; and, (iii) it is relatively labile, exchanging very fast during ligand exchange reactions. The Zn-binding sites in proteins can be classified as: (i) sites which mainly play a catalytic role; (ii) those which have a regulatory role; and, (iii) sites that have a structural role. In this latter case, the effects in proteins can vary from the fact that the sole addition of the ion causes the folding of otherwise a completely natively-unfolded protein [38], to changes in protein stability [39].

It has been known for a long time that Zn^{2+} is necessary to proper activity of hydantoinases [1,2], but its effect on either the structure or stability of the enzyme has never been explained. We have tried to address such issues by using the tetrameric dihydropyrimidinase from *Sinorhizobium meliloti,* SmelDhp, as a model. In this work, we observed that the presence of the ion leads to: (a) increase of the percentage of secondary structure (as shown by far-UV CD and FTIR); (b) changes in the environment of aromatic residues (near-UV); and, (c) changes in the stability of the protein. The increase in stability led to stabilization of the quaternary structure, as shown by the variation in the [GdmCl]$_{1/2}$-values of the first transition (Figs. 7A, B and 8A, B); this increase also explains why we have been able to obtain good crystals *only* in the presence of the ion [14]. The presence of the zinc, however, did not alter the quaternary structure (oligomerization state) of the protein (Fig. 5 A) nor did the solvent-exposure of hydrophobic polypeptide patches. But, we do not know whether the stabilized secondary structure was flickering (and then, spectroscopically-silent) when no ion was present, or alternatively, the presence of the ion induced a completely new type of structure. We favour the first explanation, since the thermodynamical parameters governing monomer unfolding (and hence, their stability) were neither altered by pH (Table 1) nor by the presence of the ion (Figs. 7 and 8) suggesting that the monomeric species had the same ASA. To the best of our knowledge, this is one of the few examples where such selective effect of Zn^{2+} on the secondary structure of a protein, but not on its quaternary one, is described.

4.2. The pH-denaturation of SmelDhp

The burial of hydrophobic residues in SmelDhp in the absence of Zn^{2+} occurred at pH 6.0, as shown by ANS, and the protein remained native-like until pH 9.0. However, the secondary structure in the absence of Zn^{2+} (as monitored by far-UV CD) was not acquired until pH 7 (Fig. 4 B, filled squares), and small tertiary rearrangements occurred at physiological pH (Fig. 3 A, blank squares). On the other hand, in the presence of Zn^{2+}, the acquisition of tertiary (fluorescence) and secondary (far-UV CD) structure occurred concomitantly at pH 6.0, without observable rearrangements in the structure (Figs. 3 C, and 4 B, blank squares). Since the pK_a of the transition in the absence of the ion, was close to that of a histidine residue (6.8±0.1) [29], we suggest that the CD conformational changes in the absence of zinc (Fig. 4 B) are related to the presence of a chelating histidine. In the X-ray structure

of tetrameric SmelDhp, His56, His58, the carboxylated-methylated Lys147, His180, His236 and Asp313 are chelating two zinc ions (PDB number: 3DC8); then, His56, His58, His180 and His236 are the most plausible residues to explain that titration. Some of those histidines might be also responsible for the changes in the <λ> of ANS experiments when zinc was present (Fig. 3 D).

The acquisition of quaternary structure, as shown by gel-filtration measurements, occurred at pH 4.0 (Fig. 5 B), whether or not the ion was present. Then, in SmelDhp, the tetrameric assembly occurred firstly, and lately conformational rearrangements, allowed acquisition of the fully native functional structure, involving the tetramer (Fig. 5 B) and the monomers (Figs. 3 and 4). All these data suggest that the complete and total acquisition of native-like features, coming from acidic solutions, occurs at similar pHs, where the maximum of the protein activity is observed; in fact, the protein is fully active in the pH range from 6.0 to 9.0 (SMR, unpublished results). Then, although some of the products and reagents used during the enzymatic reaction are not very soluble at those pHs, the possible industrial applications of SmelDhp must keep in mind that slight changes in the acidic solution conditions result in conformational changes which reduce its activity.

The acquisition of tertiary native-like structure from the acidic regions happens with a pK_a of ~4.8 (Fig. 3 A), whether or not the ion is present. This value is similar to that observed for an aspartic and/or glutamic residue [29]. Since the species present at low pH are monomeric (as shown by size exclusion chromatography (Fig. 5 B)) we hypothesize that the glutamic and/or aspartic residues involved in the acidic denaturation are also involved in the tetrameric interface. Close inspection of X-ray structure of the dimer of dimers SmelDhp shows two principal interfaces, with several Asp and Glu residues: (i) the first interface is involved in dimer assembly (with 2000 Å^2 of buried area), where Asp160, Asp161, Glu203 and Asp274 from one monomer are hydrogen-bonded to the corresponding residues in the counterpart monomer; and, (ii) the second interface is related to the formation of the dimer of dimers, with an interface area of approximately 1200 Å^2 (which should be 2400 Å^2 in total), where Asp14 and Glu360 are involved in a hydrogen-bonding network (PDB number: 3DC8). Site-directed mutagenesis experiments are underway in our laboratories to find out which particular Asp and/or Glu residues are involved in the acidic denaturation.

One final question, however, must be answered: which is the conformational state populated at low pH in the absence of the ion? Since the protein was bound to ANS (Fig. 3 B), and it did not show a sigmoidal thermal-denaturation (Fig. 2 F) in the absence of the ion, we suggest that the low-pH species is a molten-globule [40]. In the presence of the ion, probably a molten-globule-like species is present, although it has more structure, as shown by the thermal sigmoidal behaviour (Fig. 2 F), as it has been observed in other molten globules [40].

4.3. Equilibrium unfolding of SmelDhp involves a non-native monomeric intermediate whether or not zinc ions are present

Most of the previous work on protein folding has focused on small single-domain proteins that fold rapidly and avoid aggregation [41]. However, there are many proteins in the cell which are large, with multiple folding domains and/or subunits, and which probably do not follow the simple folding principles established on results from small proteins. Further complications arise in multimeric proteins, where their folding involves not only intramolecular interactions but also intermolecular ones. Moreover, the stability and folding mechanism of a protein can be altered by the presence of cofactors. It is estimated than more than 20% of all proteins in the cell coordinate cofactors in their native states to attain specific functions. Whether or not a cofactor stabilizes the protein depends on the particular polypeptide chain. For instance, the cytochrome b562 of *E. coli* is stabilized by 14 kJ mol^{-1} when the heme cofactor is present [42,43], but the stability of

the flavodoxin of *Desulfovibrio desulfuricans* was not affected by the presence of flavin [44].

The chemical-denaturations of SmelDhp showed two transitions (Figs. 7 and 8) whether or not Zn^{2+} was present. The first transition was concentration-dependent, but the second one, occurring at high GdmCl concentrations (~ 2 M), was concentration-independent. These data suggest that the first transition involves tetramer dissociation, M_4, towards a monomeric species, M: $M_4 \rightleftharpoons 4M$. The first transition cannot be a second-order step yielding dimeric structures: $M_4 \rightleftharpoons 2M'_2$ (as it could be thought from the dimer of dimers geometry of the tetramer, PDB number: 3DC8), since then, the second transition should be concentration-dependent, which was not detected in the concentration range explored (1 to 5 μM).

The structure of the monomeric intermediate is non-native, because the CD signal changed concomitantly to the fluorescence spectra (Figs. 7 and 8), under both conditions. Moreover, when GdmCl-denaturation is followed by ANS fluorescence, the decrease in either the intensity at 480 nm or the $\langle \lambda \rangle$ only occurred when the second transition had completely finished (i.e., at [GdmCl] > 3 M) (data not shown), suggesting that the monomeric intermediate species have a large amount of solvent-exposed hydrophobic surface. Further support to the non-native structure of the monomeric intermediate comes from the measurement of the ASA. The change in ASA (ΔASA) upon unfolding is related to the *m*-value by: m (J mol^{-1} M^{-1}) = 4.18×(859+0.22 (ΔASA)) [45]. The *m*-value is, on average, 17 J mol^{-1} M^{-1} (Table 1), which would yield a ΔASA = 15186 Å^2. Since the ΔASA of each monomer is 17804 Å^2 (PDB number: 3DC8), then the monomeric species exposed a rather smaller amount of ASA upon unfolding, than should be expected from a well-folded monomer. Finally, since this intermediate species is able to bind ANS (data not shown) and is monomeric, we hypothesize that its structure is similar to that of the molten-globule observed at acidic pHs.

Tetramer dissociation showed a hysteresis behaviour, whether or not the ion was present, precluding any thermodynamical study of the first transition (Fig. 7 C). Hysteresis is due to the non-equivalence of the unfolding and refolding, since the unfolding and folding processes are too slow to allow equilibrium to be established within the experimental incubation times. Then, it seems that the presence of the ion in the refolding buffer is not enough to accomplish monomer assembly in SmelDhp, even after long incubation times (data not shown). In other enzymes, the covalently-bond metallic centers only dissociate after long incubation times in unfolding conditions, allowing reversible formation of the oligomers [46]. However, the Zn^{2+} coordination in SmelDhp occurs *via* the weaker cation-π interactions, which could disrupt upon protein unfolding, and, then, they are not able to guide/allow the refolding of the protein.

4.4. Energetics of the chemical- and thermal-unfolding reaction of SmelDhp compared to other proteins

Thermal denaturations at any pH were irreversible, which could not be explained by following a model as a simple two-state irreversible model with first-order kinetics [21–23]. Further, since the dissociation reaction followed by chemical-denaturations was not reversible (and we have not been able to determine the dissociation constant of the oligomer), we could not estimate the stability of the tetramer. However, the second-step of chemical-denaturations was reversible, allowing the comparison of the calculated thermodynamic parameters of SmelDhp with those of other proteins. The dissociation free energy of other tetrameric proteins such as SecB (an α+β-protein), lactose repressor (an α-protein), peanut and soybean agglutinin (a β-protein), concanavalin A or β-glycosidase (see [47] and references therein) are in the range of 37 to 250 kJ mol^{-1} of oligomer. The global free energy of unfolding for the four non-native monomeric SmelDhp proteins is on average 150 kJ mol^{-1} (=4×17×2.2) (Table 1). This is just in the middle of the range observed for the free energy of dissociation of other proteins, which means that most of the

global free energy of unfolding in SmelDhp originates within each monomer, and the interactions establishing the tetramer scaffold, although abundant in number (as concluded from the X-ray structure: 3DC8), are relatively weak. Then, it seems that oligomerization in SmelDhp is not a key factor to attain conformational stability.

Appendix A. Supplementary data

Supplementary data associated with this article can be found, in the online version, at doi:10.1016/j.bpc.2008.10.003.

References

[1] S.H. Nam, S.H. Park, H.S. Kim, Evolutionary relationship and application of a superfamily of cyclic amidohydrolase enzymes, Chem. Rec. 5 (2005) 298–307.
[2] C.M. Seibert, F.M. Raushel, Structural and catalytic diversity within the amidohydrolase superfamily, Biochemistry 44 (2005) 6383–6391.
[3] C. Syldatk, O. May, J. Altenbuchner, R. Mattes, B. Siemann, Microbial hydantoinases-industrial enzymes from the origin of life? Appl. Microbiol. Biotechnol. 51 (1999) 293–309.
[4] J. Abendroth, K. Niefind, D. Schomburg, X-ray structure of a dihydropyrimidinase from *Thermus* sp. at 1.3 Å resolution, J. Mol. Biol. 320 (2002) 143–156.
[5] Y.H. Cheon, H.S. Kim, K.H. Han, J. Abendroth, K. Niefind, D. Schomburg, J. Wang, Y. Kim, Crystal structure of D-hydantoinase from *Bacillus stearothermophilus*: insight into the stereochemistry of enantioselectivity, Biochemistry 41 (2002) 9410–9417.
[6] Z. Xu, Y. Liu, Y. Yang, W. Jiang, E. Arnold, J. Ding, Crystal structure of D-hydantoinase from *Burkholderia pickettii* at a resolution of 2.7 Angstroms: insights into the molecular basis of enzyme thermostability, J. Bacteriol. 185 (2003) 4038–4049.
[7] K. Matsuda, S. Sakata, M. Kaneko, N. Hamajima, M. Nonaka, M. Sasaki, N. Tamaki, Molecular cloning and sequencing of a cDNA encoding dihydropyrimidinase from the rat liver, Biochim. Biophys. Acta 1307 (1996) 140–144.
[8] Z. Gojkovic, L. Rislund, B. Andersen, M.P. Sandrini, P.F. Cook, K. Schnackerz, J. Piskur, Dihydropyrimidine amidohydrolases and dihydroorotases share the same origin and several enzymatic properties, Nucleic Acids Res. 31 (2003) 1683–1692.
[9] S. Martínez-Rodríguez, F.J. Las Heras-Vázquez, J.M. Clemente-Jiménez, L. Mingorance-Cazorla, F. Rodríguez-Vico, Complete conversion of D,L-5-monosusbtituted hydantoins with a low velocity of chemical racemization into D-amino acids using whole cells of recombinant *Escherichia coli*, Biotechnol. Prog. 18 (2002) 1201–1206.
[10] A.I. Martínez-Gómez, S. Martínez-Rodríguez, J.M. Clemente-Jiménez, J. Pozo-Dengra, F. Rodríguez-Vico, F.J. Las Heras-Vázquez, Recombinant polycistronic structure of hydantoinase process genes in *Escherichia coli* for the production of optically pure D-amino acids, Appl. Environ. Microbiol. 73 (2007) 1525–1531.
[11] J. Altenbuchner, M. Siemann-Herzberg, C. Syldatk, Hydantoinases and related enzymes as biocatalysts for the synthesis of unnatural chiral amino acids, Curr. Opin. Biotechnol. 12 (2001) 559–563.
[12] J. Ogawa, S. Shimizu, Industrial microbial enzymes: their discovery by screening and use in large-scale production of useful chemicals in Japan, Curr. Opin. Biotechnol. 13 (2002) 367–375.
[13] K.P. Brooks, E.A. Jones, B.D. Kim, E.G. Sander, Bovine liver dihydropyrimidine amidohydrolase: purification, properties, and characterization as a zinc metalloenzyme, Arch. Biochem. Biophys. 226 (1983) 469–483.
[14] S. Martínez-Rodríguez, L.A. González-Ramírez, J.M. Clemente-Jiménez, F. Rodríguez-Vico, F.J. Las Heras-Vázquez, J.A. Gavira, J.M. García-Ruiz, Crystallization and preliminary crystallographic studies of the recombinant dihydropyrimidinase from *Sinorhizobium meliloti* CECT4114, Acta Crystallogr., F 62 (2006) 1223–1226.
[15] C.N. Pace, Determination and analysis of urea and guanidine hydrochloride denaturation curves, Methods Enzymol. 131 (1986) 266–280.
[16] C.N. Pace, J.M. Scholtz, Protein structure, in: T.E. Creighton (Ed.), How to determine the molar absorbance coefficient of a protein, 2nd ed., Oxford University Press, 1997, pp. 253–259.
[17] A. Hinkle, A. Goranson, C.A. Butters, L.S. Tobacman, Roles for the troponin tail domain in thin filament assembly and regulation. A deletional study of cardiac troponin T, J. Biol. Chem. 274 (1999) 7157–7164.
[18] A.F. Carvalho, J. Costa-Rodrigues, I. Correia, J.C. Costa-Pessoa, T.Q. Faria, C.L. Martins, M. Fransen, C. Sá-Miranda, J.E. Azevedo, The N-terminal half of the

peroxisomal cycling receptor Pex5p is a natively unfolded domain, J. Mol. Biol. 356 (2006) 864–875.

[19] P.J. Darlin, J.M. Holt, G.K. Ackers, Coupled energetics of lambda cro repressor self-assembly and site-specific DNA operator binding I: analysis of cro dimerization from nanomolar to micromolar concentrations, Biochemistry 39 (2000) 11500–11507.

[20] M.I. Muro-Pastor, F.N. Barrera, J.C. Reyes, F.J. Florencio, J.L. Neira, The inactivating factor of glutamine synthetase, IF7, is a "natively unfolded" protein, Protein Sci. 12 (2003) 1443–1454.

[21] J.M. Sánchez-Ruiz, J.L. López-Lacomba, M. Cortijo, P.L. Mateo, Differential scanning calorimetry of the irreversible thermal denaturation of thermolysin, Biochemistry 27 (1988) 1648–1652.

[22] F. Conejero-Lara, P.L. Mateo, F.X. Aviles, J.M. Sánchez-Ruiz, Effect of Zn^{2+} on the thermal denaturation of carboxypeptidase B, Biochemistry 30 (1991) 2067–2072.

[23] M.L. Galisteo, P.L. Mateo, J.M. Sánchez-Ruiz, Kinetic study on the irreversible thermal denaturation of yeast phosphoglycerate kinase, Biochemistry 30 (1991) 2061–2066.

[24] F.X. Schmid, Protein structure, in: T.E. Creighton (Ed.), Optical spectroscopy to characterize protein conformation and conformational changes, 2nd ed., Oxford University Press, 1997, pp. 261–297.

[25] C.A. Royer, Protein stability and folding, in: B.A. Shirley (Ed.), Fluorescence spectroscopy, Humana Press, Totowa, New Jersey, 1995, pp. 65–89.

[26] J. Backmann, G. Schäfer, L. Wyns, H. Bönisch, Thermodynamics and kinetics of unfolding of the thermostable trimeric adenylate kinase from the archaeon *Sulfolobus acidocaldarius*, J. Mol. Biol. 284 (1998) 817–833.

[27] I. Echabe, J.A. Encinar, J.L.R. Arrondo, Removal of spectral noise in the quantitation of protein structure through infrared band decomposition, Biospectroscopy 3 (1997) 469–475.

[28] Y.P. Zhang, R.N. Lewis, R.S. Hodges, R.N. McElhaney, FTIR spectroscopic studies of the conformation and amide hydrogen exchange of a peptide model of the hydrophobic transmembrane alpha-helices of membrane proteins, Biochemistry 31 (1992) 11572–11578.

[29] R.L. Thurlkill, G.R. Grimsley, J.M. Scholtz, C.N. Pace, pK values of the ionizable groups of proteins, Protein Sci. 15 (2006) 1214–1218.

[30] G.V. Semisotnov, N.A. Rodionova, O.I. Razgulyaev, V.N. Uversky, A.F. Gripas, R.I. Gilmanshin, Study of the "molten globule" intermediate state in protein folding by a hydrophobic fluorescent probe, Biopolymers 31 (1991) 119–128.

[31] R.W. Woody, Circular dichroism, Methods Enzymol. 246 (1995) 34–71.

[32] S.M. Kelly, N.C. Price, The use of circular dichroism in the investigation of protein structure and function, Curr. Prot. Pept. Sci. 1 (2000) 349–384.

[33] S. Vuilleumier, J. Sancho, R. Loewenthal, A.R. Fersht, Circular dichroism studies of barnase and its mutants: characterization of the contribution of aromatic side chains, Biochemistry 32 (1993) 10303–10313.

[34] A. Barth, S.R. Martin, P.M. Bayley, Resolution of Trp near UV CD spectra of calmodulin-domain peptide complexes into the ^1L_a and ^1L_b component spectra, Biopolymers 45 (1998) 493–501.

[35] T.E. Creighton, Proteins, Structures and molecular properties, 2nd ed., W. H. Freeman, New York, 1993.

[36] J.M. Berg, H.A. Godwin, Lessons from zinc-binding peptides, Annu. Rev. Biophys. Biomol. Struct. 26 (1997) 357–371.

[37] A.J. Thomson, H.B. Gray, Bio-inorganic chemistry, Curr. Opin. Chem. Biol. 2 (1998) 155–158.

[38] S. Yi, B.L. Boys, A. Brickenden, L. Konermann, W.Y. Choy, Effects of zinc binding on the structure and dynamics of the intrinsically disordered protein prothymosin alpha: evidence for metalation as an entropic switch, Biochemistry 46 (2007) 13120–13130.

[39] P.S. Park, K.T. Sapra, M. Kolinski, S. Filipek, K. Palczewski, D.J. Muller, Stabilizing effect of Zn^{2+} in native bovine rhodopsin, J. Biol. Chem. 282 (2007) 11377–11385.

[40] O.B. Ptitsyn, Molten globule and protein folding, Adv. Protein Chem. 47 (1995) 83–229.

[41] S.E. Jackson, How do small single-domain proteins fold? Fold. Des. 3 (1998) R81–R91.

[42] C.R. Robinson, Y. Liu, J.A. Thomson, J.M. Sturtevant, S.G. Sligar, Energetics of heme binding to native and denatured states of cytochrome b_{562}, Biochemistry 36 (1997) 16141–16146.

[43] P. Wittung-Stafshede, J.C. Lee, J.R. Winkler, H.B. Gray, Cytochrome b_{562} folding triggered by electron transfer: approaching the speed limit for formation of a four-helix-bundle protein, Proc. Natl. Acad. Sci. U. S. A. 96 (1999) 6587–6590.

[44] D. Apiyo, J. Guidry, P. Wittung-Stafshede, No cofactor effect on equilibrium unfolding of *Desulfovibrio desulfuricans* flavodoxin, Biochim. Biophys. Acta 1479 (2000) 214–224.

[45] J.K. Myers, C.N. Pace, J.M. Scholtz, Denaturant m values and heat capacity changes: relation to changes in accessible surface areas of protein unfolding, Protein Sci. 4 (1995) 2138–2148.

[46] D. Apiyo, K. Jones, J. Guidry, P. Wittung-Stafshede, Equilibrium unfolding of dimeric desulfoferredoxin involves a monomeric intermediate: iron cofactors dissociate after polypeptide unfolding, Biochemistry 40 (2001) 4940–4948.

[47] S. Sinha, N. Mitra, G. Kumar, K. Bajaj, A. Surolia, Unfolding studies of soybean agglutinin and concanavalin A tetramers: a comparative account, Biophys. J. 88 (2005) 1300–1310.